Development of an Efficient Photocathode CuO/Sb_2S_3 Heterojunction for Photoelectrochemical Water Splitting

A Thesis

Submitted to

Indian Institute of Science Education and Research Pune in partial fulfillment of the requirements for the BS-MS Dual Degree Programme

by

Aishwarya Singh

Indian Institute of Science Education and Research Pune
Dr. Homi Bhabha Road,
Pashan, Pune 411008, INDIA.

April, (2023).

Supervisor: Prof. Ch. Subrahmanyam

Aishwarya Singh

Certificate

This is to certify that this dissertation entitled " Development of an efficient Photocathode CuO/Sb_2S_3 Heterojunction for Photoelectrochemical Water Splitting " towards the partial fulfillment of the BS-MS dual degree program at the Indian Institute of Science Education and Research, Pune represents study/work carried out by Aishwarya Singh at Indian Institute of Technology, Hyderabad under the supervision of Prof. Ch. Subrahmanyam, Professor, Chemistry department" during the academic year 2022-23.

Prof. Ch. Subrahmanyam

Committee :

Prof. Ch. Subrahmanyam

This thesis is dedicated to my Parents and my Siblings for their endless affection and their dedicated involvement for success in my life

Declaration

I hereby declare that the matter embodied in the report entitled " Development of an efficient Photocathode CuO/Sb_2S_3 Heterojunction for Photoelectrochemical Water Splitting " are the results of the work carried out by me at the Department of Chemistry, Indian Institute of Technology (Hyderabad), under the supervision of Prof. Ch. Subrahmanyam and the same has not been submitted elsewhere for any other degree.

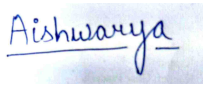

Aishwarya Singh

Date- 31/03/2023

Table of Contents

List of Figures

List of Tables

Abstract

Developing an efficient photocathode system from the earth's abundant materials is essential for effectual Photoelectrochemical (PEC) water splitting. The charge transfer between heterojunctions is important in fabricating a novel composite, keeping cost-effectiveness, abundance, and PEC performance in mind. The p-type narrow band gap photocathode, CuO synthesized by hydrothermal method, was decorated with Sb_2S_3 by adopting the facile Chemical Bath Deposition (CBD) procedure to fabricate CuO/Sb_2S_3 heterojunction. The heterojunction shows better PEC performance contrary to the exposed CuO Photocathode. The improvement in the photocurrent density (J_{ph}) of CuO/Sb_2S_3 with respect to CuO is due to the enhanced charge carrier generation and separation of the electron and holes. The composite CuO/Sb_2S_3 shows a higher J_{ph} value (-1 $mA.cm^{-2}$) than CuO (-0.3 $mA.cm^{-2}$) photoelectrode at 0 V_{RHE} in the 0.5 M Na_2SO_4 (pH 6.85). Sb_2S_3 works as a sensitizer, diminishing the recombination rate of the e^-/h^+ in the CuO photocathode. UV-Visible spectroscopy shows CuO/Sb_2S_3 composite with enhanced absorption spectrum compared to pristine CuO and Sb_2S_3 films. The photoluminescence (PL) emission spectra indicate less charge carrier recombination in the case of CuO/Sb_2S_3. As well as the Electrochemical impedance spectroscopy (EIS) studies show less charge transfer resistance in the case of CuO/Sb_2S_3 than CuO. This finding can help in developing new photocathodic materials with the composite of Cu-based binary oxides and chalcogenides, which is challenging to synthesize due to certain inbuilt restrictions with the materials and the experimental constraints.

Acknowledgments

I am grateful to Prof. Ch. Subrahmanyam for his assistance throughout the project. His expertise and knowledge in the research field steered me in the right direction. His feedback was the primary factor for the successful completion of the project. I am honored to have had the opportunity to work under the supervision of such a dedicated and talented person. The experience I gained in my MS Thesis will benefit my future endeavors.

Many thanks to Prof. Nirmalya Ballav (Expert) for his contributions to the project. His guidance and support have been essential in the completion of the thesis as well as the mentorship, and the lessons I gained through his collaboration were most valuable for me.

I thank my mentor, Mohit Kumar (Ph.D. Scholar), for his support throughout the journey.

The instrumental facilities of the Indian Institute of Technology (IIT), Hyderabad, allowed me to conduct my research with precision and accuracy. I am thankful to the Lab assistant and whole staff members who provide the facilities commonly to each student. The opportunity to use such a high–quality resources played a significant role in my work.

At last, an evident appreciation for my family, friends, and lab members for their support and contributions throughout this project. Great thanks to everyone whom I mentioned above, as well as to everyone whom I missed to include.

Chapter 1

Introduction

1.1 Background :

Photoelectrochemical (PEC) water splitting is the technology that uses sunlight to power a chemical reaction that separates water into hydrogen and oxygen. The exciting part of this clean, renewable, and sustainable method is the evolution of hydrogen gas. Hydrogen in the future can replace fossil fuels. It will help meet the demand of the energy crisis and the environmental problem through which the world is going on in the current scenario [1]. As most artificial systems mimic natural systems, natural photosynthesis is the primary root for the emergence of the manufactured system of water splitting with the role of sunlight. Photosynthesis is an essential biochemical process that produces biological oxygen molecules (O_2) and H_2 or H_2-related species from the water as a substrate. The phenomenon includes a two-step excitation process in which the oxidation and reduction half-reactions are spatially separated and proceeded in Photosystem II (PS-II) and Photosystem I (PS-I), respectively [2]. The active site is contained within a larger protein complex, where the complex is composed of four manganese ions and one Ca^{2+}.

In early 1971, Fujishima and Honda's research showed that TiO_2 could decompose water under PEC conditions. This was revolutionary work in the field of artificial photosynthesis [3].

$$2H^+ + 2e^- \longrightarrow H_2(g) \qquad (\text{HER: } H_2 \text{ evolution reaction})$$

$$2H_2O \longrightarrow O_2 + 4H^+ + 4e^- \qquad (\text{OER: } O_2 \text{ evolution reaction})$$

Overall: $2H_2O \rightarrow O_2 + 2H_2$ (light condition) $\Delta E° = -1.23$ V ($\Delta G° = 237.18$ kJ mol^{-1})

The positive $\Delta G°$ value stipulates that water splitting is a non-spontaneous reaction; hence, additional energy should be provided to drive the process. Here the required energy is given in the form of sunlight.

1.2 Principle of PEC water splitting :

PEC water splitting involves creating electron-hole pairs within a semiconductor material, specifically on photocathodes and photoanodes, through the absorption of light. These photogenerated charge carriers are then transferred to the juncture between the semiconductor and electrolyte, where they can be used to facilitate the hydrogen evolution reaction (HER) and the oxygen evolution reaction (OER), respectively. The semiconductors selected must possess a band gap that exceeds 1.23 eV . The ionic-conductivity loss in the electrolyte and overpotential loss should be considered. Hence, the actual potential requirement exceeds 1.6 eV [4]. These semiconductors are known as photocatalysts, and the phenomenon associated with this is photocatalysis. The main disadvantage of photocatalysis is that H_2 and O_2 will evolve on the same surface. Hence, we cannot quantify the gases, and here the advantage of the electrochemical system exists.

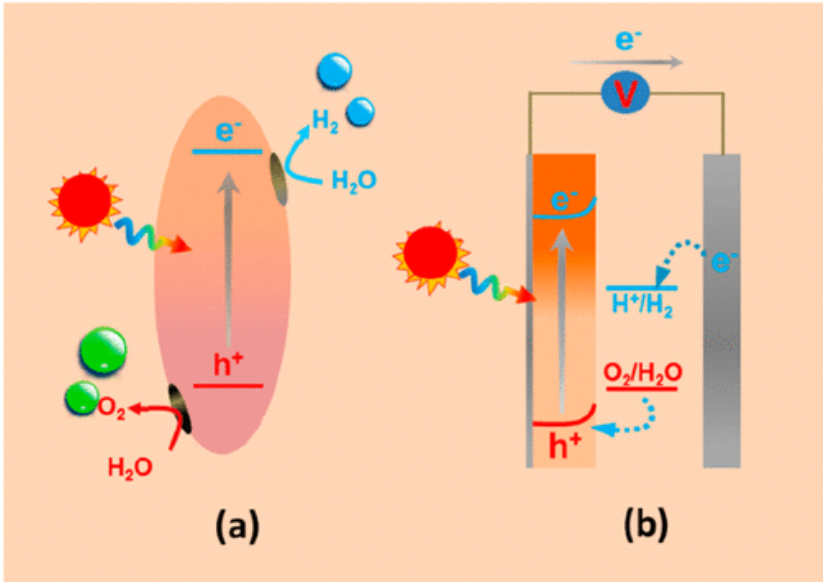

Figure 1: (a) Schematic for the photocatalysis phenomenon, (b) Schematic of the photoelectrochemical Water splitting. Copyright © 2022, American Chemical Society.

The other advantage of the electrochemical system is the possibility of overcoming the problem of charge recombination due to band bending. In order for the semiconductor/electrolyte interface to be in a state of equilibrium, their electrochemical potentials must be equal. The electrochemical potential of the solution is determined by the redox-potential of the electrolyte. On the other hand, the redox-potential of the semiconductor is determined by the Fermi-level position. In a practical system, the energy levels of the

redox potential in the solution and the Fermi level are not the same. This difference in energy levels allows for the transfer of charges between the electrolyte solution and the semiconductor. For p-type semiconductors, the redox potential of the electrolyte solution is higher than the Fermi level.

Consequently, electrons move from the electrolyte side to the photocathodes to establish balance. As a result, the photocathode side becomes negatively charged, while the electrolyte side becomes positively charged. Creating an electric field that results in downward bending [5]. The inverse effect occurs in n-type photoanodes. Space-charge region facilitates the separation of electrons and holes. V_{fb}, or flat band potential, is a necessary term that describes the potential where the band energy level is flat. It measures photoanode/photocathode electrochemical potential in relation to the electrolyte. Exposure of semiconductors to visible light leads to stimulation of electron from the valence band (V.B) to the conduction band (C.B), resulting in a minor change in the concentration of holes, the primary charge carriers in photocathodes. As a result, the quasi-Fermi level of the holes remains constant, whereas the concentration of electrons significantly increases. This increase causes a consequential difference in the quasi-Fermi level in light and dark conditions, resulting in photovoltage. The extent to which the band's bend dictates the photovoltage [6].

1.3 Properties of semiconductor materials in PEC Water splitting :

However, factors like photo-corrosion, poor efficiencies, sluggish reaction kinetics over the surface, and lack of suitable material for photoelectrodes limit today's PEC water splitting applications. There are various steps that can be implemented to enhance the effectiveness of PEC water dissociation: (1) the band gap positioning should be optimized. (2) narrow band-gap semiconductors capable of harvesting visible light should be used (3) charge carrier separation and transfer should be improved (4) the materials used for PEC water splitting should be stable and light-resistant.

Photoanodic materials are well explored in the literature with several material modification and fabrication techniques compared to photocathodic materials. Our primary interest is the HER, associated with photocathodic (p-type semiconductors) materials. Charge carrier recombination and photo corrosion pose problems for photocathodic materials. Various strategies are used to address these issues: controlling the morphology [9], controlled doping, modification with elements [10], fabricating facile heterojunction [11], adding 2-D materials [12], incorporating protective/passivation layer, interlayers like buffer layer and hole

transport layer (HTLs) [13], decorating cocatalyst [14], etc. Protective layers are also used to overcome the problem of surface states. The position of the Fermi level at the surface of an interface between a semiconductor and an electrolyte is not fixed but rather fluctuates with the electrochemical potential of the electrolyte. This allows maximum bending of the energy bands at the point of contact. The surface states, or chemisorption phenomenon, result in states within the gap that pin the Fermi level. When the regular pattern of the lattice terminates at the surface, electronic states are formed, which are referred to as surface states. These states are generally within the semiconductor's band gap, which increases the possibility of an electron being transferred from the conduction band to these states rather than being involved in the H_2 evolution.

Because of their excellent conductivity, p-type metal oxides (Cu-based binary/ ternary oxides) as photocathodes are the best candidates as absorber materials. However, they are unstable because light-induced e^-/h^+ can participate in the reduction of Copper as the reduction potential value lies within the band-gap of the material. Cu-based ternary oxides are more stable as compared to the binary oxides making the ternary oxides more advantageous to be used as photocathodes. The general formula for these oxides can be represented in the form of $CuMO_2$, where M is any other transition metal. The ternary oxides inhibit Cu $3d^{10}$ to 4s excitation because the transition from Cu $3d^{10}$ to the empty orbitals of the other transition metal is more favored, which allows the material to be stable. These oxides have less photoconversion efficiency because of diverse factors, such as inappropriate surface quality and high density of surface states (DOS) present in the material. Some modifications can be made to make the material more efficient: Oxygen intercalation to the Cu layer or using the host-guest approach in the formation of the whole system etc.

1.4 Copper-based oxides suitable for PEC:

Several Copper based materials are well-explored as p-type photocathodes in literature. Among them, Cu_2O is the most investigated one. The crystal structure of the material is simple cubic with a unit cell containing four copper atoms and two oxygen atoms. The theoretical prediction of the photocurrent density (J_{ph}) for Cu_2O is ~ -14 $mA.cm^{-2}$ with 18% photoconversion efficiency [15]. In contrast, photodegradation and recombination rates limit its ability to be used as photoactive material. To overcome these problems, Al-doped ZnO, Ga_2O_3 buffer layer, TiO_2, etc., are used as a protection layer. Cocatalysts such as RuO_x, SnO_2, MoS_x, and NiFe-layered double hydroxide have been integrated with Cu_2O photocathodes to

enhance the overall effectiveness of the material. [16].The most recent and efficient system with $Cu_2O/Ga_2O_3/TiO_2/RuO_x$, nanowire photocathode reveals a J_{ph} of -10 mA cm^{-2} at 0 V_{RHE} for 120 h [17]. Cu_2O has inherent limitations because of the wide band gap (E_g = 2eV). This limits the light-harvesting property of the material to only up to 600 nm wavelength.

Due to its low band gap of 1.2–1.5 eV, CuO is a well-liked photocathodic material because it can absorb a considerable percentage of the solar spectrum. Unfortunately, CuO possesses high defect density and poor heterojunction interface quality [18][19]. Some investigations have concentrated on techniques including doping, plasmonic metal, nanostructure introduction, and CuO crystallinity and stoichiometric composition management. The creation of a $CuO/CdS/TiO_2$/Pt photocathode resulted in a stable photocurrent of 1.68 $mA.cm^{-2}$ lasting for 30 minutes at 0 V_{RHE}. On the other hand, $CuO/ZnO/TiO_2$/Au-Pd produced a system with a photocurrent of -5.3 $mA.cm^{-2}$ at 0 V_{RHE} and photostability of 87% after 5 hours [20].

Due to enhanced photostability and charge transfer, the heterojunction produced between Cu_2O, a direct band gap semiconductor, and CuO, an indirect band gap semiconductor, has recently attracted much attention. Ni has vigorous electrocatalytic activity, as evidenced by studies on the Cu_2O/CuO/Ni heterojunction, which produces a J_{ph} of -4.3 $mA.cm^{-2}$ at 0 V_{RHE} [21]. The Cu_2O/CuO system, modified using Cu_2S-Pt, is another heterojunction that has drawn attention for its quick hydrogen evolution. Charge transfer was made more accessible, and recombination was avoided using Cu_2S and Pt as cocatalysts. A photocurrent density of -5.7 $mA.cm^{-2}$ at 0 V_{RHE} was seen in the resulting $Cu_2O/CuO/Cu_2S$/Pt system, which was 2.5 times greater than that seen for the Cu_2O/CuO heterojunction.[21]. Due to the development of recombination sites and the absorption of undesired light, an excessive amount of Cu_2S deposition decreased photocurrent density. [22]. A back contact material is required to avoid recombination and enable charge transfer, and Au is the best option because of its Surface Plasmon Resonance (SPR) feature. Metal nanoparticles have inherent SPR properties, and photocathodes containing sandwiched metal nanoparticles have shown the potential to boost the performance of PEC cells. The fabrication of p-Cu_2O/AuAg/n-Cu_2O increases the concentration of charge carrier, resulting in the system with high onset potential, E_{op} (~0.8 V_{RHE}), as compared to the homojunction p-Cu_2O/n-Cu_2O (E_{op} = 0.7 V_{RHE}) and p-Cu_2O (E_{op}= 0.43 V_{RHE}) [23].

The ternary oxides with earth-abundant constituents are also explored in the literature. $CuFeO_2$'s delafossite phase has a narrower E_g, measuring at 1.5 eV. The other attractive advantage of $CuFeO_2$ is that the photocathode surface is reasonably active for CO_2 reduction. From ultraviolet to infrared, $CuFeO_2$ is a substance that can absorb a variety of electromagnetic spectrum bands. A photocurrent of -2.4 $mA.cm^{-2}$ at 0 V_{RHE} has been observed by intercalating oxygen and altering with Ni-Fe layer double hydroxide/Reduced graphene oxide electrocatalysts [24]. Magnesium incorporation is another method to improve the conductivity and carrier concentration of $CuFeO_2$ besides oxygen intercalation. Due to its large E_g value of about 3.5 eV, $CuAlO_2$ can be used as an affordable mesoporous structure for $CuFeO_2$.For oxygen reduction, it was discovered that the FTO/$CuAlO_2$/$CuFeO_2$ configuration produces J_{ph} of -2.4 $mA.cm^{-2}$ at 0.4 V_{RHE}, which is 2.4 times higher than that of the FTO/$CuFeO_2$ configuration [25]. Preventing the formation of other phases like CuO, Fe_2O_3, and $CuFe_2O_4$ during the synthesis process is the main challenge in producing single-phase $CuFeO_2$. Moreover, the inadequate PEC activity of $CuFeO_2$ is related to the recombination caused by defect states present in bulk or on the surface.

$CuBi_2O_4$ is a p-type material that possesses E_g value of approximately 1.6-1.8 eV and has a tetragonal crystal structure with square planar $Cu(II)O_4$ groups that are stacked together and linked to the trigonal polyhedra of distorted $Bi(III)O_6$ [26]. The investigation of the electronic structure of $CuBi_2O_4$ discloses that the V.B and C.B edges of the material are formed through a combination of Cu 3d and O 2p orbitals. However, the efficiency of the $CuBi_2O_4$ photocathode is constrained by inadequate optical absorption and insufficient charge carrier transport within the material. To overcome these limitations, one approach is to nanostructure the material. Another possibility is incorporating a back contact layer between the FTO and $CuBi_2O_4$-based photocathodes, which can significantly enhance the overall PEC performance. In experiments, introducing NiO as FTO/NiO/$CuBi_2O_4$ layer has demonstrated a 50% improvement in photocurrent compared to the bare photocathode. Additionally, using Cu-doped NiO as a HTL (Cu: NiO) has shown promise in enhancing the photocurrent. In this scenario, a photocurrent of -2.83 mA cm^{-2} at 0.6 V_{RHE} can be achieved when an H_2O_2 electron scavenger is present [27]. Different heterojunctions were fabricated such as $CuBi_2O_4/BiVO_4$, $CuBi_2O_4$/CuO, $CuBi_2O_4$/CdS/TiO_2 ,$CuBi_2O_4$/AgI, $CuBi_2O_4$/ZnSe/TiO_2 etc. to ameliorate the overall execution of $CuBi_2O_4$ photocathodes.

Theoretical studies predict the great potential of ternary-based oxides in artificial water splitting. Despite that, these materials are associated with a number of experimental

problems. Ternary-based oxides often require a high-temperature annealing procedure to create the appropriate phase, which may cause the absorber and bottom electrodes (in this case, FTO) to degrade as a result of interdiffusion. Furthermore, because many of these oxides contain multivalent transition metals, secondary phase problems could arise. Hence, several practical constraints and material-related issues must be taken into account in order to effectively construct electrodes employing phase pure ternary-based oxides.

1.5 Copper-based chalcogenides suitable for PEC:

In the previous decades, several materials have been explored in the field of artificial photosynthesis. P-type Copper-based chalcogenides have been emerging materials according to recent literature due to the earth's abundance, narrow band gap, adequate absorption coefficient, and facilitated charge transport properties. Due to their higher half-cell solar-to-hydrogen (HC-STH) efficiency, which has grown to 8.5%, these materials are more appealing for PEC hydrogen production. Their stability has been shown to last up to 20 days without a substantial drop in photocurrent, adding to their allure. In the binary sulfides, Cu_2S and CuS are the most explored materials. Ternary-based sulfides have the advantage of wide light absorption, fast charge-carrier dynamics, and, most crucial appropriate energy band structure. The S 3p orbital's smaller positive charge in its valence band than the O 2p orbital is the main cause of the intrinsic characteristics. Photoactive material such as $CuSbS_2$, $CuFeS_2$, $CuInS_2$, $CuGaS_2$, Cu_2ZnSnS_4,Cu_2BaSnS_4, $CuInGaS_2$ are quite emerging. The problem of recombination centers due to photostability and crystal defects is also associated with Cu-based chalcogenides. One of the major issues with sulfides is their susceptibility to leaching under extreme conditions.

Cu_2S (Eg = 1.6-2 eV) has a high absorption coefficient. Several synthesis processes, such as hydrothermal, annealing, hot injection method, sulfurization, electrodeposition, etc., are already in the literature. The system formed with $Cu_2S/CdS/TiO_2/RuO_x$, where RuO_x works as a cocatalyst, gives the remarkable photocurrent of -7 mA cm^{-2} at -0.3 V_{RHE} with E_{op}=0.48 V_{RHE} [28].

$CuInS_2$ is a photoactive material with a narrow band gap ranging from 1.5 to 1.8 eV used in solar cells and PEC applications. However, one of the most significant disadvantages of this material is its proclivity for recombination. Thus, there is a need to have modifications with another material. The deposition of the HTL works efficiently to enhance the performance of $CuInS_2$ [29]. The FeOOH/$CuInS_2$/Pt system gives J_{ph} value of -6 mA cm^{-2} at -0.4V_{RHE} [30].

Various heterojunction which increases overall performance efficiency, such as $CuInS_2$/CdS/Pt, $CuInS_2$/In_2S_3/Pt, $CuInS_2$/CdS/MoS_2, $CuInS_2$/SnS_2/$C_{60,}$ etc., are well studied in the literature.

Additionally, the $CuSbS_2$ photocathode is quite attractive in PEC water splitting. The material crystallizes into the orthorhombic chalcostibite-type structure, where Cu and Sb atoms occupy cation sites in an alternating fashion. In addition, four S atoms collaborate with both Cu and Sb atoms.$CuSbS_2$ has been used for the hole extraction to prevent the recombination, and it shows the temperature-dependent band gap (E_g = 1.57 -1.58 eV). The J_{ph} of 0.35 mA cm^{-2} at 0.9 V_{RHE} is obtained by the system Fe-$Zn_{0.2}Cd_{0.8}S$/$CuSbS_2$/Co-Pi because of multiple synergistic effects. However, the sample gets corroded to 94% after 1.6 h, even with less photocurrent [31]. Remarkable photocurrent density (J_{ph} = -18 mA cm^{-2}) at 0 V_{RHE} in the supporting electrolyte of 1M H_2SO_4 is obtained with the hybrid system of $CuSbS_2$/Sb_2Se_3/TiO_x/Pt photocathode. Another study shows the facile heterojunction formation of $CuSbS_2$ and CdS, here $CuSbS_2$/CdS/Pt gives J_{ph} = -4.1 mA cm-^{2} at 0 V_{RHE} with E_{op} = 0.45V_{RHE} [32].

Photocathodes based on quaternary copper sulfides are a novel development that warrants further investigation. However, the two major problems with these materials are that they are stable in narrow phases, and the existence of secondary phases leads to poor PEC performance. Copper chalcopyrite-based Cu(In, Ga)SSe (CIGS) is a highly studied material in solar cells, with E_g ranging from 1.0 to 1.7 eV and an efficiency of up to 20%. [33]. Various study shows the achievement of high photocurrent (18-27 mA cm^{-2}) with CIGS and $CuGaSe_2$ photocathodes in 0.5 M H_2SO_4 solution [34]. Two approaches can be used to improve the efficiency of CIGS: incorporating a solid-state p-n junction to facilitate charge separation and using a catalyst to promote surface reactions.

Cu_2ZnSnS_4 (CZTS) is another emerging p–type material that can be synthesized by electrodeposition, molecular ink, hydrothermal, vacuum-based synthesis, etc. [35]. The disorder in the Cu/Zn lattice structure causes the energy bands to broaden, a phenomenon known as band tailing, which limits the material's performance. [36]. The early reports showing the fabrication of Mo/Cu_2ZnSnS_4/CdS/AZO/TiO_2/Pt gives Jph > 1 mA/cm^2 at 0 V_{RHE}. The upconversion nanoparticles (UCNPs) are used for converting the near Infrared region (NIR) light into visible light, which makes visible spectrum absorptive photocathodes absorb NIR light as well. The insertion of UCNPs in the CZTS photocathodes gives an

appreciable J_{ph} value of -4 mA/cm^2 under the illumination of 980 nm light at 0 V_{RHE}. The utilization of upconversion nanoparticles (UCNPs) as a converter of near-infrared (NIR) energy has the potential to escalate the Solar to Hydrogen (STH) conversion efficiency [37]. The comparison of CdS and In_2S_3 as a buffer layer was investigated with CZTS photocathodes. The result shows higher J_{ph} with In_2S_3. Additionally, Cu_2BaSnS_4 is a better material than CZTS due to the replacement of Zn with Ba [38][39]. Due to the significantly greater ionic size of Ba2+, the CBTS Phase has a much wider chemical potential range than the CZTS Phase.

1.6 Sb_2S_3 as an effective sensitizer :

The literature shows that the formation of heterojunction needs proper band alignment between the materials; along with that, there is a need for a buffer layer or sensitizer, cocatalyst, etc., to increase the overall efficiency. The fabrication of the oxides-sulfides hybrid system is quite challenging compared to oxides-oxides and sulfides-sulfides due to several practical obstacles. As discussed, the Copper based binary/ternary oxides or sulfides base material needs different supporting materials (NiO, ZnO, CdS, In_2S_3, Sb_2Se_3, etc.) to overcome the inbuilt problems related to the base material. CdS is the most explored sensitizer, significantly improving the base material's properties. Due to its poisonous qualities, using CdS in several applications puts people and animals in danger. In contrast, In_2S_3 can perform the same function as CdS without endangering living things. In_2S_3 is a superior buffer layer over CdS. However, it could not be economical for industrial applications. Sb_2S_3, which is less expensive and non-toxic, is another choice. Due to the van der Waals interaction between the stacked Sb_4S_6 ribbons, Sb_2S_3 is a one-dimensional semiconductor that displays anisotropic behavior in various directions. Due to its high absorption coefficient (>10^5 cm^{-1}) and narrow band-gap (1.5-1.8 eV), this material exhibits tremendous promise in the field of photovoltaics, notably in the construction of heterojunctions with inorganic semiconductors [40]. The fabrication of $Sb_2S_3/TiO_2/Pt$ heterojunction gives the photocathodic current of -3 mA.cm^{-2} at 0 V_{RHE}. The E_{op} occurred earlier when In_2S_3 was utilized as a buffer layer between TiO_2 and Sb_2S_3 [41]. There are reports on the formation of heterojunction of Sb_2S_3 with ternary Copper based photocathodes, but only a few with binary Copper based photocathodes.

Sb_2S_3, $CuSbS_2$, or $NaSb_5S_8$ can be inserted to enhance the growth of $Cu_2ZnSn(S, Se)_4$ grains. Facilitating the creation of a large grain CZTSSe absorber thin film is crucial to promoting

the mobility of photogenerated carriers and reducing grain boundary recombination. The crystal growth is maximum with Sb_2S_3 than with $CuSbS_2$ and atlast with $NaSb_5S_8$ (Sb_2S_3 > $CuSbS_2$> $NaSb_5S_8$) [42] . The reason for selecting materials containing Sb-based elements is that they can assist grain growth during the process of selenization, which ultimately leads to the fabrication of a pure-phase CZTSSe photocathode.

$CuInS_2$ efficiency can be improved by fabricating a novel $CuInS_2/In_2S_3$ heterojunction, where Pt is used as a cocatalyst ($CuInS_2/In_2S_3$/Pt). This hybrid photocathode gives J_{ph} = -2.48 mA.cm^{-2} at -0.6 V_{RHE}. The value of J_{ph} is about 3.13 times higher than compared to bare $CuInS_2$ photoelectrode (J_{ph}= -0.79 mA cm^{-2} at -0.6 V_{RHE}). Additionally, $CuInS_2/Sb_2S_3$ heterojunction with the appropriate band positioning results in broadening the retaliation range to the visible spectrum and increasing the separation/transfer rate of charge carriers.[43].

The operation of Sb_2S_3 to form a heterojunction with $CuBi_2O_4$, while plasmonic Au nanoparticles were sandwiched in between these two materials. The photocathode fabrication as $CuBi_2O_4$/Au/Sb_2S_3 gives Jph = -3.2 mA.cm^{-2} at 0 V_{RHE}, pH 6.65, directing to a two-fold increase, compared to bare $CuBi_2O_4$ (Jph = -1.5 mA.cm^{-2} at 0 V_{RHE}) [44].

The composite of Copper based binary oxides with Sb_2S_3 needed to be explored more. In this study, we created a novel FTO/CuO/Sb_2S_3 composite to upgrade the effectiveness of CuO. CuO is incredibly unstable, as was previously mentioned. Even though CuO has many benefits, it has challenges with the fabrication of heterojunction with any photoactive material having proper band alignment. Both CuO and Sb_2S_3 have a small band gap. Despite that, this heterojunction works efficiently due to the better electron transfer from the CuO side to Sb_2S_3, resulting in improved charge separation and a decrease in the possibility of recombination rate. This leads to the enhanced photocurrent and photovoltage of the photocathodic system. Due to the similar band gap of CuO and Sb_2S_3, the recombination rate of the composite cannot be reduced to a much greater extent. Hence there is a need to add some cocatalyst or Plasmonic nanoparticles to the mentioned heterojunction so that the overall performance can be enhanced significantly. The fabrication of the heterojunction (FTO/CuO/Sb_2S_3) is presented in this thesis work with the evidence of the improved performance of CuO with the addition of sensitizer (Sb_2S_3).

Chapter 2

Material and Methods

2.1 Synthesis of CuO powder :

CuO powder was synthesized by modifying the previously reported method [45]. The reagent used for the synthesis were: $CuCl_2.2H_2O$ (Copper(II) chloride dihydrate, Avra), NaOH (Sodium hydroxide, SRL), and deionized (DI) water. The solution was prepared from 0.43 g of $CuCl_2.2H_2O$ in 5 ml of DI water; then, it was blend with 5 M NaOH (25 ml) solution, followed by stirring for about 30 minutes. The mixture was then placed in a hydrothermal reactor and maintained at 140˚C for 24 hours. Afterward, the formed black precipitate was separated through centrifugation and washed multiple times using a mixture of DI water and ethanol. The obtained precipitate was subsequently dried and annealed for an hour at a temperature of 500°C.

2.2 Fabrication of the CuO electrode :

The Doctor Blading technique was used to fabricate the FTO/CuO photocathodic electrode. To make the CuO slurry, 10 mg of powder was mixed with 2-3 drops of ethylene glycol (EG). The slurry was sonicated for 15-20 min and then heated at 500°C to evaporate the EG solvent.

2.3 Fabrication of CuO/Sb_2S_3 electrode :

The Sb_2S_3 layer over CuO was composed by the chemical bath deposition method (CBD) [46]. The procedure for synthesizing Sb_2S_3 was taken from the existing literature, with some modifications. The reagents used for the synthesis were: $SbCl_3$ (Antimony (III) chloride, Sigma Aldrich), $Na_2S_2O_3.5H_2O$ (Sodium thiosulphate pentahydrate, Fisher Scientific), acetone, and DI water. To create the bath for Sb_2S_3, a mixture of 195 mg of $SbCl_3$ and 0.75 ml of acetone (Solution A) was prepared to ensure the complete dissolution of the $SbCl_3$. Afterward, 7.5 ml of a 0.3 M solution of $Na_2S_2O_3.5H_2O$ was added to Solution A, followed by sonication for 15-20 minutes. The obtained transparent solution gives pH = 3.5. Afterward, 21.75 ml of water was put on to make the volume up to 30 ml. The solution's color shifts from a clear hue to an orange shade, indicating the creation of the Sb_2S_3 complex. 0.3M $Na_2S_2O_3.5H_2O$ and DI water was maintained at 10°C before adding it to the $SbCl_3$ mixture. The CuO photocathode was deposited for 5 h into the bath with the coated phase

towards the wall of the beaker. The coated films were washed with DI water + ethanol. To achieve the crystalline phase of Sb_2S_3, the FTO/CuO/Sb_2S_3 films were subjected to annealing at 400°C for one hour while being surrounded by an argon atmosphere. The Sb_2S_3 synthesis from CBD can be explained as follows. The reaction of $SbCl_3$ and $Na_2S_2O_3.5H_2O$ gives a complex of antimony thiosulfate ($Sb_2(S_2O_3)_3$); this, after hydrolysis, turns into Sb_2S_3 [47]. In the acidic medium (pH ~3.5), The hydrolysis of $(S_2O_3)^{2-}$ was preceded by the decomposition of the intermediate complex ($Sb_2(S_2O_3)_3$) to produce Sb^{3+} and S^{2-}, which reacted to form Sb_2S_3. The following reaction formula can describe it.

$$Sb_2(S_2O_3)_3 + 3H^+ + 6e- \longrightarrow Sb_2S_3 + 3HSO_3^-$$

Characterization techniques for Photocathodic materials

2.4 UV–visible spectroscopy (UV-Vis) :

UV-Vis spectroscopy was utilized in conducting optical studies on the fabricated films, and this was done to examine their absorption characteristics. The equation for the absorption coefficient, which is measured in units of m^{-1}, can be expressed as follows.

$$(\alpha h\nu) = A(h\nu - E_g)^{m}$$

This equation relates the absorption coefficient of a material to its direct and indirect band gaps, where m is a constant value of ½ or 2 depending on the type of band gap. By plotting the square of (αhν) versus hν, the direct band gap can be determined by extrapolating the linear region. On the other hand, the square root of (αhν) versus hν plot evaluates the indirect band. The constant A is used to scale the data appropriately.[48].

2.5 Flat band potential (V_{fb}) :

V_{fb} determines the energy level at which the band is flat. It is related to the measurement of photocurrent onset potential, V_{on}. However, the Mott-Schottky method is more efficient for obtaining V_{fb}. The assumption used in this method is that altering the applied potential (V_{app}) results in a modification of the width of the space-charge region, and the capacitance change follows the Mott-Schottky relationship, as shown below [49].

$$\frac{1}{C_{SC}^2} = \left(\frac{2}{\varepsilon\varepsilon_0 en}\right)\left(V - V_{fb} - \frac{k_B T}{e}\right)$$

The ε represents the dielectric constant, while ε_0 is the permittivity of the free space, and V denotes the applied potential. k_BT/e can be neglected as it is relatively small at room

temperature. Hence, from the above equation, V_{fb} can be calculated from the intercept of C_{SC}^{-2} vs. axis that measures the potential. By analyzing the linear portion of the Mott-Schottky plot, one can obtain information about the sample's carrier concentration (n).

2.6 Linear sweep voltammetry (LSV):

LSV is used for measuring the PEC activity of the material. The study utilized a three-electrode configuration. The reference electrode is a saturated Ag/AgCl electrode, the counter electrode is made of Pt, and the working electrode is our photoactive material. During Linear Sweep Voltammetry (LSV), the voltage gradually increased from the lower to the upper limit. The working electrode's potential was adjusted to a reference point of the Reversible Hydrogen Electrode (RHE). To achieve this conversion, the equation specified in the reference was employed [50].

$$E_{RHE} = E_{Ag/AgCl} + 0.059V \times pH + E^{\circ}_{Ag/AgCl}$$

Where $E^{\circ}_{Ag/AgCl}$ = 0.1976 V (reference electrode), pH: pH of the electrolyte solution, $E_{Ag/AgCl}$: Applied potential in working mode.

2.7 Electrochemical Impedance Spectroscopy (EIS) :

EIS is the technique used for the investigation of the properties of the material and the electrode reactions. A sinusoidally varying potential (V_{ω}) is applied across the sample in the impedance analysis. The resultant time-dependent current (I_{ω}) is measured as the function of the frequency. Z is a vector that combines two separate scalar properties: resistance and reactance. It measures the opposition to the flow of alternating current (AC) in a system comprising resistance, capacitance, and inductance. The impedance can be measured over the range of frequency using this technique. EIS data is either displayed as a complex quantity (Nyquish plot) or vector (Bode plot). When representing impedance using a Nyquist plot, the real part of the impedance (Z') is plotted against the imaginary part (Z''). The Nyquish plot of impedance gives a semicircle, where the radius of the semicircle represents the contact and charge resistance of the electrodes [51].

2.8 X-Ray Diffraction :

This technique gives the understanding of the structures, preferred crystal orientation, Phases, Crystallinity, and crystal defects of the material. Bragg's equation can define the interference pattern of X-rays scattered by crystals.

$$n\lambda = 2d\sin\theta$$

The interplanar spacing (represented by d) can be determined using the incident X-ray wavelength (λ), the order of reflection (n), and the angle of incidence (θ) [52].

2.9 Photoluminescence Spectroscopy (PL) :

In photoluminescence (PL), three primary stages are involved: excitation, relaxation, and emission. The PL spectra are utilized to investigate how photoinduced charge carriers move and recombine, providing significant insights into the optical and photochemical features of photoactive materials. To gain a thorough understanding of the semiconductor's electronic structure and interfacial point defects, PL is crucial. However, the major disadvantage of this technique is its destructive nature when the systems undergo reactions in the excited state, leading to limitations in its application [53].

2.10 Scanning Electron Microscopy Analysis (SEM) :

SEM gives 3-D images of a sample with high resolution with the help of a beam of electrons in a raster scan pattern. There are various ways to create high-energy electron beams, including tungsten filaments and field emission weapons. The beam is produced, accelerated using high voltage, and pointed at the sample. The electrons carry significant kinetic energy as they go through the sample. The Kinetic energy is dissipated as a variety of signals when electron-sample interaction takes place. The secondary electrons associated with the signals play a significant role in obtaining the morphology. The orientation and crystal structure of the sample can be determined by utilizing diffracted backscattered electrons.

2.11 X-ray photoelectron Spectroscopy (XPS) :

XPS gives information about the elements, their oxidation state, and coordination number in the material. By measuring the kinetic energy of photoelectrons emitted from atoms on the material's surface, the counts per second (eV) can be obtained as a function of their kinetic energy. This allows the electronic state of atoms in the sample to be characterized by observing variations in electron intensity at different emission energies. It can also give quantifiable information about surface composition.

Chapter 3

Result and Discussion

3.1 Crystallographic Studies (XRD) :

Powder XRD was considered to examine the crystallographic nature of the fabricated films (CuO, Sb_2S_3, CuO/Sb_2S_3). The wavelength used for the X-ray was ~ 0.154 nm for Cu Kα. The PXRD pattern of the CuO films showed an End-centered lattice with a Monoclinic crystal system having the cell parameters of a = 4.688 Å, b = 3.422 Å, and c = 5.131 Å. The peaks of the crystal can be obtained at 2θ = 32.50°, 35.54°, 38.71° , 48.72°, 53.48°, 58.26°, 61.52°, 66.22°, 68.12° with the most intense peak at 2θ = 38.71°.

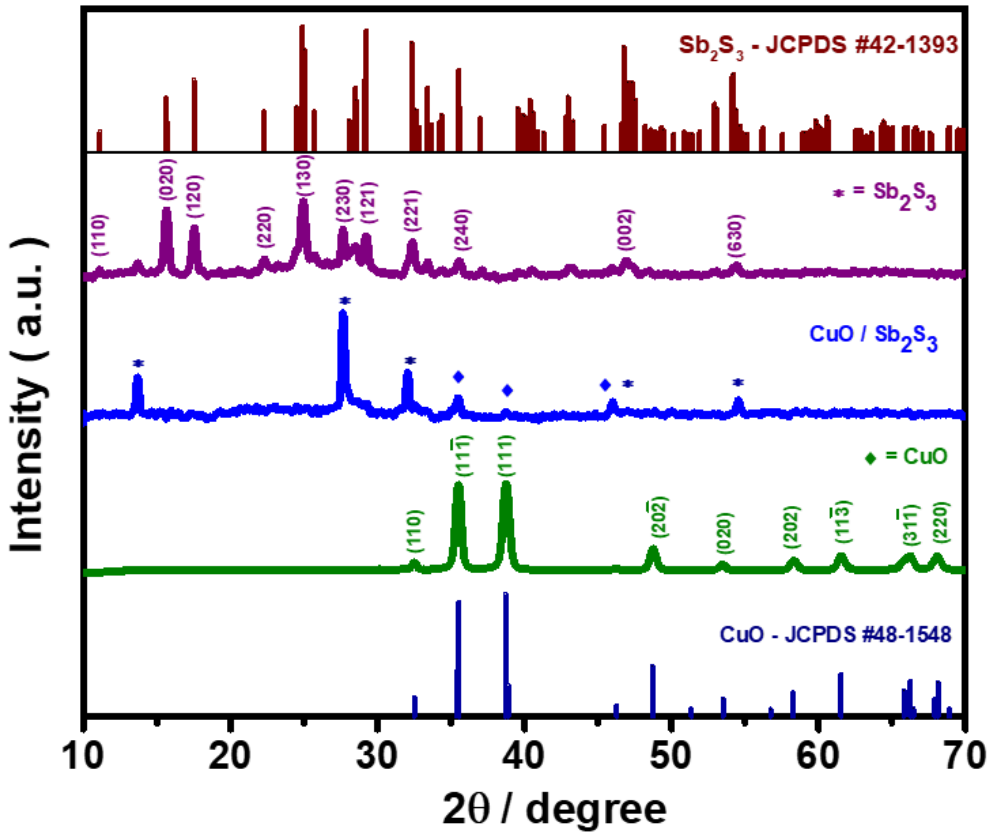

Figure 2: PXRD pattern of CuO (♦) with JCPDS data (#48-1548), CuO/Sb_2S_3 composite photoelectrode, and Sb_2S_3 (*) with the JCPDS data (#42-1393).

The d values corresponding to the mentioned 2θ values are 2.75, 2.52, 2.32, 1.87, 1.71, 1.58, 1.50, 1.41, 1.37 Å having the alignment with the planes (110), $(11\bar{1})$, (111), $(20\bar{2})$, (020), (202), $(11\bar{3})$, $(31\bar{1})$, (220), respectively. The pattern matches well with the JCPDS card #48-1548. While the fabricated Sb_2S_3 films showed a Primitive lattice with the Orthorhombic crystal system, the cell parameters for Sb_2S_3 are a = 11.23 Å, b = 11.31 Å, and C = 3.841 Å. The 2θ values for these films are 11.12°, 15.64°, 17.52°, 22.28°, 24.88°, 28.48°, 29.16°, 32.35°, 35.52°, 47.30°, 54.65° correlate to the d values of 7.95, 5.66, 5.06, 3.99, 3.58, 3.13, 3.06, 2.76, 2.52, 1.92, 1.68 Å. The peaks match well with the planes (110), (020), (120), (220), (130), (230), (121), (221), (240), (002), and (630), respectively. In this case, the most intense peak is at 2θ = 24.88° corresponding to the plane of (130). CuO/Sb_2S_3 composite XRD pattern indicates the existence of both CuO (♦) and Sb_2S_3 (*), confirming the photocathode's stability.

3.2 Morphology Studies :

In order to examine the physical structure of the produced photocathodes, images were taken using a FE-SEM microscope for different configurations. FE-SEM follows the same principle as the SEM technique. The only difference is that in the case of FE-SEM, a potential gradient is applied to emit the electron beam, and SEM uses thermionic emission. Fig. 3 shows micrographs of CuO and Sb_2S_3. The CuO material synthesized by the hydrothermal process followed by doctor blading on the FTO shows Flakes morphology of various sizes, Fig. 3 (a-d). While in the case of Sb_2S_3 synthesized by the CBD method shows spherical structures

Fig. 3 (e-h).

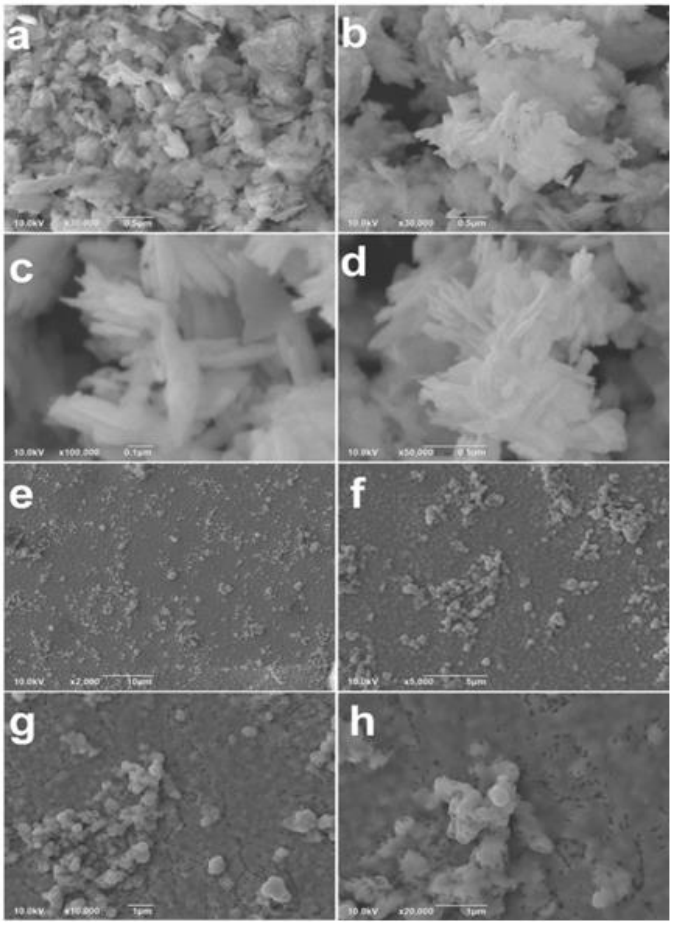

Figure 3: FE-SEM micrographs of CuO film on FTO (a-d), Sb_2S_3 films (e-h)

3.3 XPS Studies :

The chemical state of the CuO/Sb_2S_3 composite was investigated using X-ray photoelectron spectroscopy (XPS). The prepared films showed the presence of Cu, O, Sb, and S elements, as depicted in Fig. 4(a). Furthermore, Fig. 4(b-d) illustrates high-resolution XPS spectra of Cu 2p, Sb 3d, O 1s, and S 2p. Based on the information in Fig. 4(b), it is evident that the peaks observed at 933.71 and 953.87 eV correspond to Cu $2p_{3/2}$ and Cu $2p_{1/2}$, respectively. The difference in the binding energy of 20.16 eV indicates the existence of Cu^{2+}. Additionally, the presence of two satellite peaks at 942.56 and 962.21 eV may be attributed to the presence of the $3d^9$ shell of Cu^{2+}, indicating the presence of CuO. These findings are consistent with the literature. [48]. The presence of Sb^{3+} ions in Sb_2S_3 is indicated by the measured peaks at 528.50 eV (corresponding to Sb $3d_{5/2}$) and 537.50 eV (corresponding to Sb $3d_{3/2}$) [54] (Fig. 4 (C)). The peak observed for the O 1s at 529.32 eV is attributed to oxygen atoms in the lattice structure [55], and S 2p peaks at 160.10 eV (S $2p_{3/2}$) and 162.10 eV (S $2p_{1/2}$) [56] can be observed from Fig.4 (d).

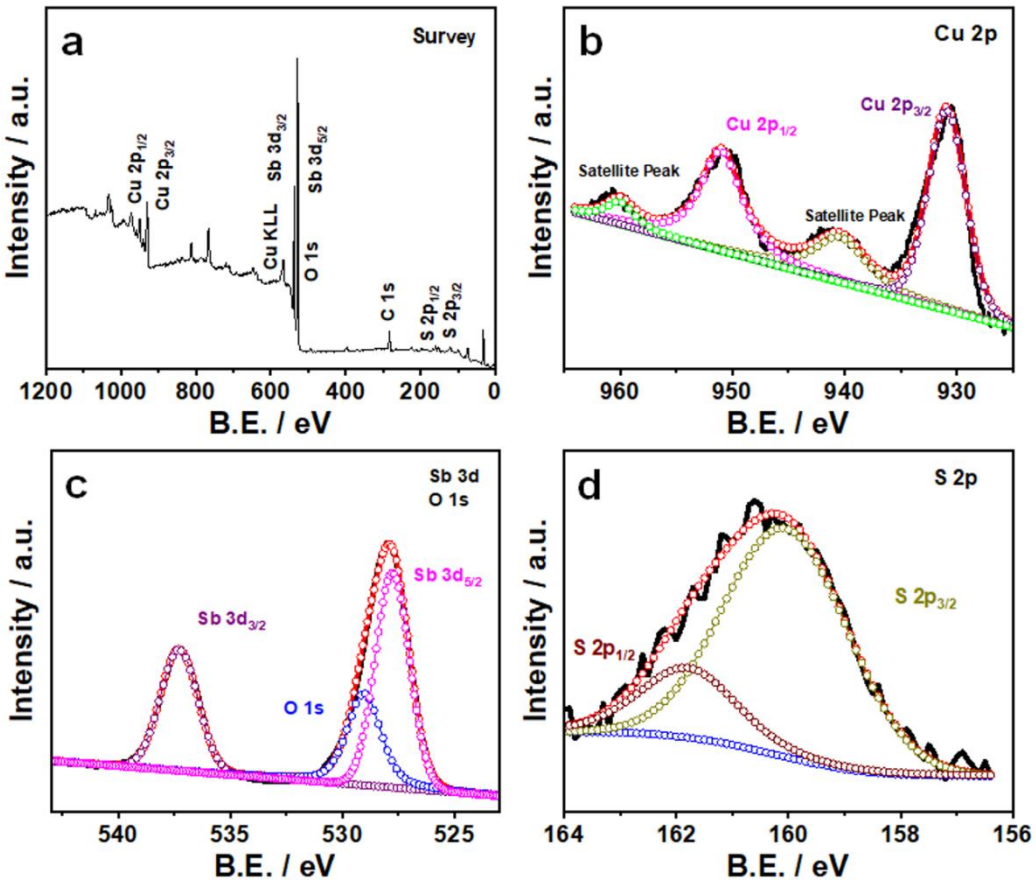

Figure 4: XPS Spectra of CuO/Sb_2S_3 films with (a) Survey Scan, HR-XPS of (b) Cu 2p, (c) Sb 3d and O 1s, and (d) S 2p.

3.4 Optical Studies :

UV-Vis spectroscopy was utilized to investigate the optical properties, absorption characteristics, and band-gap features (Fig. 5a-c). The CuO nanoflakes showed absorption in a visible region corresponding to the UV band edge emission starting at 810 nm (Fig. 5a). UV-Vis spectrum of Sb_2S_3 showed a sharp absorption peak maximum at 650 nm while the emission band edge was at 825 nm. A sharp peak was also observed in the CuO/Sb_2S_3 composite film (Fig. 5a). This CuO/Sb_2S_3 composite showed an enhanced absorption spectrum compared to pristine CuO and Sb_2S_3 films.

The band-gap calculations were performed using the experimental UV-Vis Spectroscopy data through Tauc's plot (Fig. 5b, c). The band-gap of CuO and Sb_2S_3 was calculated to be 1.56 and 1.5 eV, respectively.

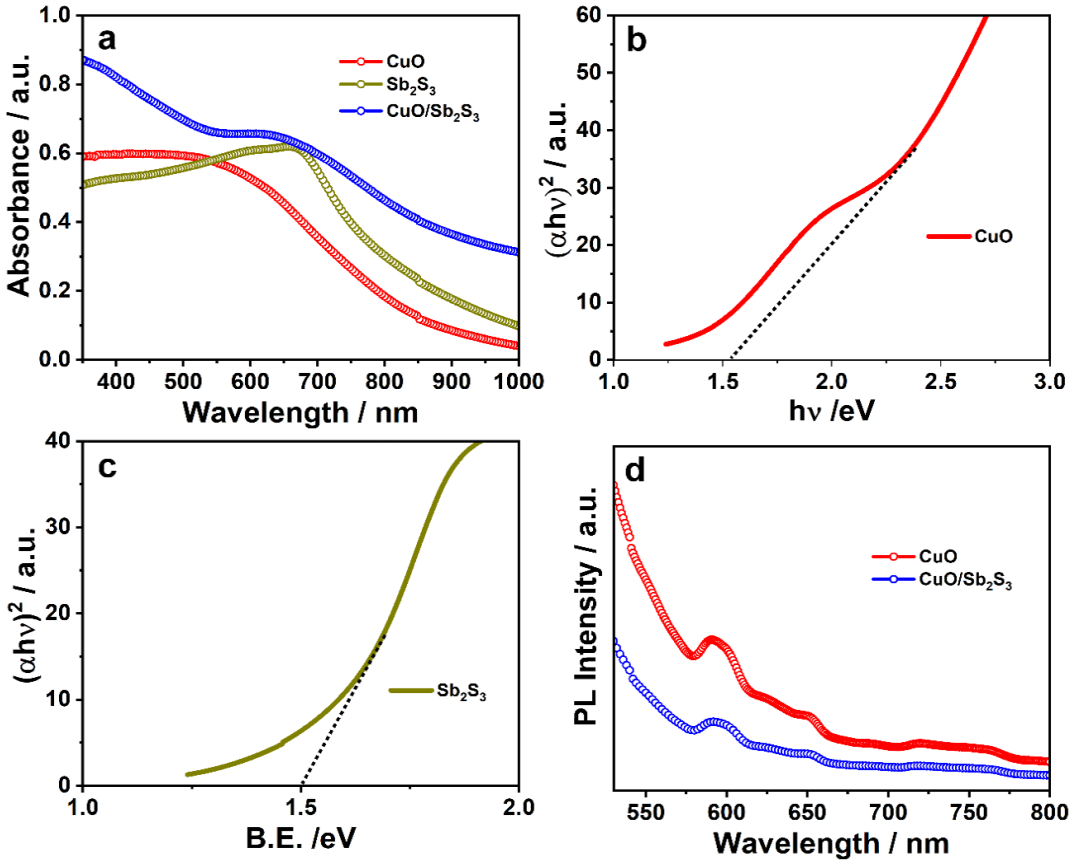

Figure 5: (a) UV-Vis spectroscopy of thin films of CuO, Sb_2S_3, and CuO/Sb_2S_3, Tauc's plot of (b) CuO, (c) Sb_2S_3, (d) steady-state photoluminescence spectra of CuO and CuO/Sb_2S_3.

Further, to investigate the characteristics of heterojunction formed between the CuO and Sb_2S_3, as well as the reduction in the rate of recombination of photogenerated charge carriers, photoluminescence spectroscopy was scrutinized (Fig. 5d).

On the excitation wavelength of 500 nm, three peaks were observed at 590 and 650, and a broad emission peak from 720-770 nm for CuO thin film. Meanwhile, when excited, CuO/Sb_2S_3 composite decreased peak intensity at 590, 650, and 720-770 nm. The reduction in strength could be explained by the effective transfer of electrons from the conduction band of CuO to the conduction band of Sb_2S_3, which occurs through a type II heterojunction-based electron transfer mechanism. The reduction in the intensity of emission also hints towards the reduced rate of recombinations that were taking place in CuO/Sb_2S_3 heterojunction compared to pristine CuO.

3.5 Photoelectrochemical Studies :

The prepared sample was tested for Water splitting by performing the photocurrent measurements under the chopped illumination of white light to examine their photoactivity. By varying the potential of the substance throughout a range of -0.2 to 0.8 V against RHE at a rate of 10 mv/sec, the substance's PEC reaction was detected in both dark and light circumstances. An electrolyte with a pH of 6.85 and a concentration of 0.5 M sodium sulfate (Na_2SO_4) was used for the measurement. The working electrode area for all the films was fixed as 0.25 cm^{-2}. The J_{ph} obtained from the LSV plot follows the Randles–Sevcik equation.

$$i_p = 0.4463\, n^{3/2} F^{3/2} A\, \frac{D^{1/2} c v^{1/2}}{(RT)^{1/2}}$$

The variable "n" in the following expression stands for the number of electrons, and "F" is the Faraday constant (with a value of 96,485 C/mol). The symbol "A" stand for the working electrode's area, "c" for the photoactive substance's concentration, "v" for scan speed, and "D" for the diffusion coefficient. The universal gas constant "R" (8.314 J/mol.K) and "T," which stands for the absolute temperature, are involved in the denominator part of the equation.

The CuO films synthesized by the hydrothermal process and the heterojunction (CuO/Sb_2S_3) synthesized by the deposition of CuO films in the Sb_2S_3 chemical bath were examined for the photoelectrochemical test, as shown in Figure 6 (a). The J_{ph} of CuO was -0.3 mA cm^{-2} at 0 V_{RHE}. Meanwhile, the J_{ph} value for CuO/Sb_2S_3 was -1 mA cm^{-2} at 0 V_{RHE}. The deposition of CuO films in the Sb_2S_3 bath was done at different time variations (5 hr, 10 hr, 15 hr). However, the 10 hr and 15 hr films were not synthesized properly due to prolonged deposition time, resulting in the peeling off of the CuO powder in the chemical bath of Sb_2S_3. As a result, after a 5-hour deposition process, the J_{ph} value significantly increased roughly three times over the unaltered CuO photocathode. Along with the enhanced J_{ph} value, the

onset potential (E_{onset}) was also observed to shift in a positive direction in CuO/Sb_2S_3 as compared to CuO only. E_{onset} is defined as the potential where the product is produced, or photoactivity is observed over the working electrode on light illumination.

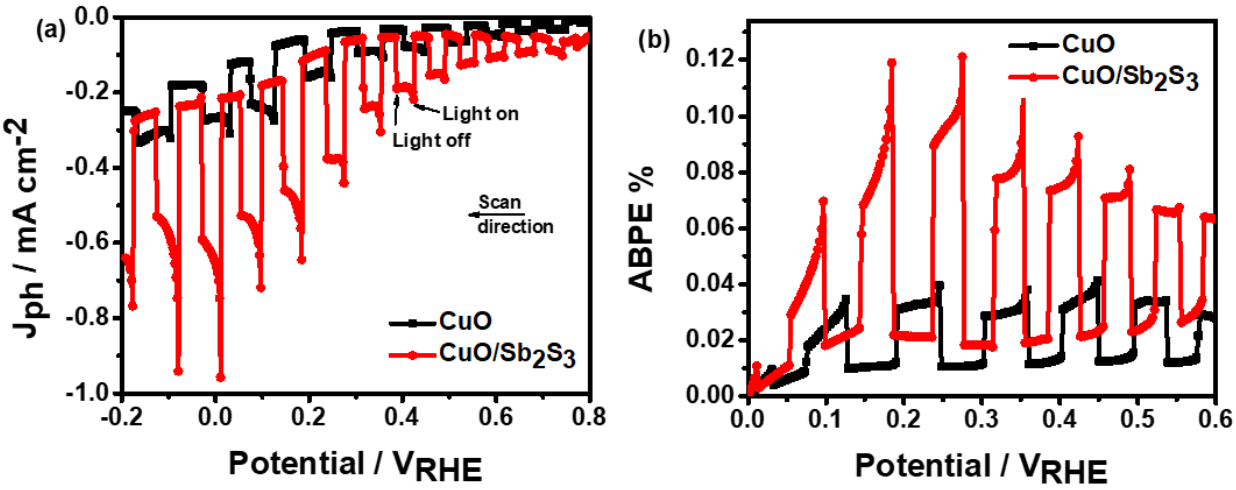

Figure 6: (a) I-E curve of CuO and CuO/Sb_2S_3 electrode under chopped illumination under AM 1.5G at the scan rate of 10 mV/sec, (b) ABPE efficiency of CuO and the composite CuO/Sb_2S_3 under the solar radiation in 0.5 M aqueous Na_2SO_4 electrolyte

For the photocathode, the higher the E_{onset}, the better the photoelectrode, and vice-versa. E_{onset} for the films followed a trend having CuO/Sb_2S_3 (0.80 V_{RHE}) > CuO >. Thus, we concluded that the CuO/Sb_2S_3 shows better photoactivity with respect to CuO. From Figure 6 (a), we can also observe that both CuO and CuO/Sb_2S_3 films show high dark currents and increase significantly in the case of CuO/Sb_2S_3. This indicates the electrons leaking to the defect states and surface states within the band gap.

The applied bias photon to current efficiency (ABPE) is calculated when the bias is applied for photoelectrolysis.

$$\text{ABPE } \%) = \left[\frac{(J_{photo})\ (\text{mA cm}^{-2}) \times (E_{rc} - E_{app})\ (\text{V})}{P_{photo}\ (\text{mW cm}^{-2})}\right] \times 100$$

E_{rc} denotes the standard cell potential for water reduction at 0 V_{RHE}, whereas P_{photo} denotes the light intensity of 100 mW cm^{-2}. The photocurrent density obtained from the photoactive material is represented by J_{photo} (mA cm^{-2}). However, the term has limitations because it depends on the applied voltage factor, which may not accurately reflect the photoconversion efficiency for PEC water splitting.

According to the data in Fig. 6 (b), the maximum ABPE efficiency for CuO and CuO/Sb_2S_3 is 0.04% and 0.10%, respectively, observed at 0.25 V_{RHE}.

3.6 Electrochemical Impedance Spectroscopy (EIS) studies :

Electrochemical impedance spectroscopy was carried out under light and dark conditions using a three-electrode setup consisting of a reference electrode made of Ag/AgCl and a counter electrode made of a Pt rod with 0.5 M Na_2SO_4 at 0 V_{RHE} and 10 mV amplitude. The apparent activity of photoelectrode can be seen in dark and light conditions. The creation of charge carriers in both light and darkness enhanced the transport of charges to the contact between the electrode and the electrolyte. (Fig. 8a).

The CuO/Sb_2S_3 photocathode showed a lower charge transfer resistance than CuO. The equivalent electrochemical circuit shown in Fig. 8b explains the charge movement across the heterojunction and electrode/electrolyte interface.

Fig.7 represents the components contributing to the overall resistance in the system, including R_S, which represents the resistance of the solution, R_1, which is the bulk resistance of the photoactive material (CuO and CuO/Sb_2S_3), C_{dl}, which stands for the capacitance of the double layer within the photoactive material, and R_2 and CPE, represents the resistance and constant phase element at the interface between the electrode and electrolyte. The fitting parameters from the theoretical equivalent circuits concerning the experimental Nyquist plots are mentioned below in Table 1.

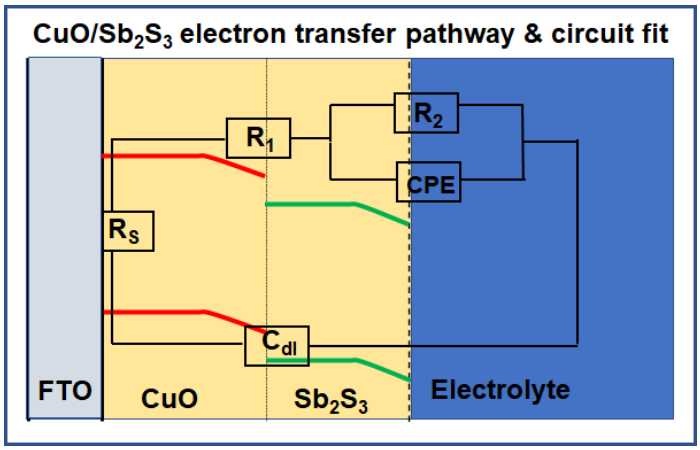

Figure 7: Electron transfer pathway and circuit fir for CuO/Sb_2S_3

Table 1: The R_S (Ω), R_1 (kΩ), C_{dl} (kF), R_2 (TΩ), and CPE (µMho*s^N, where N=0.77) value comparison of the photocathode CuO with the composite CuO/Sb_2S_3.

Photocathode	R_S (Ω)	R_1(kΩ)	C_{dl}(kF)	R_2(TΩ)	CPE(µMho*s^N)
CuO	30.7	500	76.5	1.30	115
CuO/Sb_2S_3	27.8	200	50	1.09	208

Bode-phase plots plotted between the frequency (Hz) and the phase angle (deg) give us information about the electron lifetime or time period in an electrical circuit. The frequency maximum (f_{max}) of the bode phase plot is indirectly proportional to the time period of the electron, i.e., $1/2\pi f_{max}$.

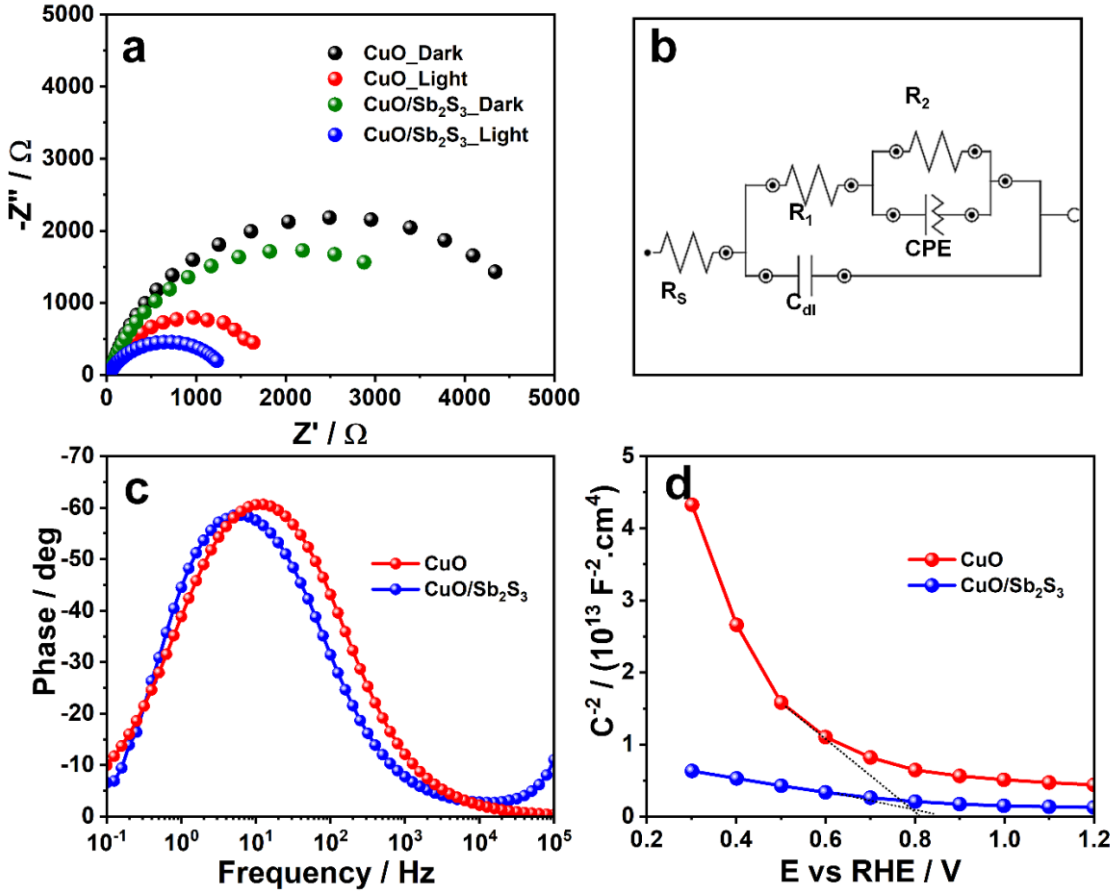

Figure 8 : (a) Nyquist plots of CuO, CuO/Sb_2S_3 in dark and light illumination conditions at 0 V_{RHE} in 0.5 M Na_2SO_4 electrolyte; (b) equivalent circuit fitted for the experimental Nyquist

plots; (c) Bode-phase plot of CuO and CuO/Sb_2S_3 photocathode; (d) Mott-Schottky plot of CuO and CuO/Sb_2S_3 photocathode.

The time period of electron for CuO and CuO/Sb_2S_3 was found to be 13 and 29 ms. The improved period hints toward efficient heterojunction formation and charge transfer. Mott-Schottky plots were plotted [C^{-2} ($F^{-2}.cm^4$) vs. E(V_{RHE})] for CuO and CuO/Sb_2S_3 photocathodes in order to visualize the band diagram and the charge transfer mechanism. CuO and CuO/Sb_2S_3 were found to have E_{FB} values of 0.82 and 0.85 V_{RHE}, respectively. The successful production of heterojunction is responsible for the rise in E_{FB}. Furthermore, the Mott-Schottky (M-S) plot slope is inversely related to the charge carrier concentration. The lower slope of CuO/Sb_2S_3 (7.82) compared to CuO (5.75) indicates the higher charge carrier concentration in the CuO/Sb_2S_3 composite photocathode.

3.7 Other possible heterojunctions with Sb_2S_3 :

NiO/Sb_2S_3 :

In this instance, mesoporous NiO nanosheets were created by spin-coating a seed layer of NiO and then doing CBD. The precursor solution made of nickel acetate, ethanol amine, and ethanol was used to create the seed layer on FTO, followed by annealing at 450°C for 1 hour in the presence of air. $NiSO_4.6H_2O$ and $K_2S_2O_8$ were combined to form a solution, which was then used to fabricate the mesoporous sheets. To maintain the pH of the bath, ammonia solution was added dropwise. The seeded substrate was then immersed in the bath for 4 h to obtain the appropriate layer thickness. The samples were then again heated to 450°C in an air environment. Following the 5 h deposition of these NiO films onto the Sb_2S_3 chemical bath, a composite material was synthesized as FTO/NiO/Sb_2S_3, where NiO is used as Hole Transport Layer (HTL).

NiO is a promising material due to its high transparency, large band gap (E_g > 3.5 eV), and cost-effectiveness. The disadvantage associated with NiO is that it has high resistivity, making the constraint in the formation of heterojunction. Additionally, NiO shows significantly less power conversion efficiency than other photocathodic materials due to high defect density and low electron mobility, resulting in a high rate of surface-mediated recombination. Hence, this can be the reason for not getting significant enhancement in the J_{ph} value of NiO/Sb_2S_3 concerning Sb_2S_3.

The bare Sb_2S_3 and NiO/Sb_2S_3 were tested for water splitting by performing the photocurrent measurements under the chopped illumination of white light. The LSV was employed to scan the potential range of -0.2 to 0.8 V (vs. RHE) under both dark and illuminated conditions at a scan rate of 10 mV/sec. The measurement was conducted using an electrolyte of 0.5 M Na_2SO_4 with a pH of 6.85. The photocathode material's working electrode area was fixed at 0.25 cm^{-2}. Fig. 9 shows that the J_{ph} for bare Sb_2S_3 was -0.48 mA cm^{-2}, while for NiO/Sb_2S_3, the J_{ph} was -0.3 mA cm^{-2} at 0 V_{RHE}, after a sudden drop from -0.5 mA cm^{-2} at 0.12 V_{RHE}. This suggests that the heterojunction was not successfully fabricated.

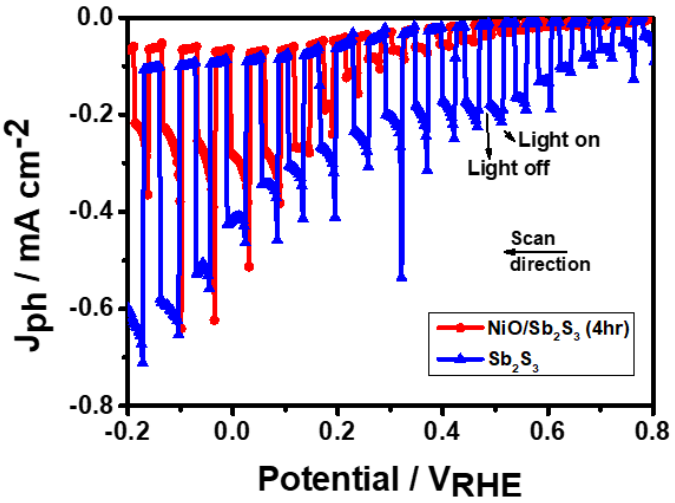

Figure 9: I-E curve of Sb_2S_3 and NiO/Sb_2S_3 electrode under chopped illumination under AM 1.5G at the scan rate of 10 mV/sec.

Cu_2ZnSnS_4(CZTS)/Sb_2S_3 :

The CZTS was fabricated by preparing the precursor solution and then spin-coating the solution on FTO to form the continuous films [58].

The substrate used for the synthesis of precursor solution is $CuCl_2.2H_2O$ (0.5 M), $ZnCl_2$ (0.25 M), $SnCl_4$ (0.25 M), and Thiourea (N_2H_4CS, 1.25 M). The solvent used for this case is 2-Methoxyethanol. The substrates were stirred for 1 hour in a water bath to form the homogeneous solution, resulting in the transparent yellow color solution. After that, the solution was coated on the FTO. For heterojunction formation ($FTO/CZTS/Sb_2S_3$), the prepared films were deposited on an Sb_2S_3 bath for 5hr. As the free sulfide ions (S^{2-}) produced by the reaction interact with the metal ions (Cu, Zn, and Sn), CZTS nuclei are created.

CZTS band gap ranges from 1.48 to 1.63 eV depending on the increase in the [Sn]/[Cu] ratio. The change in the E_g value can be accounted for by creating imperfections at low levels of Sn. Furthermore, this material is both abundant in the earth's crust and free of toxicity. The absorption coefficient value of CZTS is more significant than 10^4 cm^{-1}. Due to the proper band alignment of CZTS and Sb_2S_3, this novel approach for the heterojunction formation was analyzed. The CZTS photocathode has inbuilt disadvantages as it forms cliff-like band alignment, which leads to interface recombination.

Additionally, it results in the appearance of a large density at the interface, which is the primary factor for the minority carrier recombination at the interface. From Fig. 10, using CZTS as an HTL for Sb_2S_3 does not significantly enhance the J_{ph} value. By scanning the photocathodic material's potential between -0.2 and 0.8 V (vs. V_{RHE}) at a rate of 10 mv/Sec, the PEC response was examined in dark and lighted circumstances. The supporting electrolyte for the measurement was a phosphate buffer with a pH of 6.85, and the electrode area was maintained at 0.25 cm^{-2}. The J_{ph} at 0 V_{RHE} for CZTS was found to be -0.42 mA cm^{-2}, whereas CZTS/Sb_2S_3 showed a J_{ph} of -0.44 mA cm^{-2}.

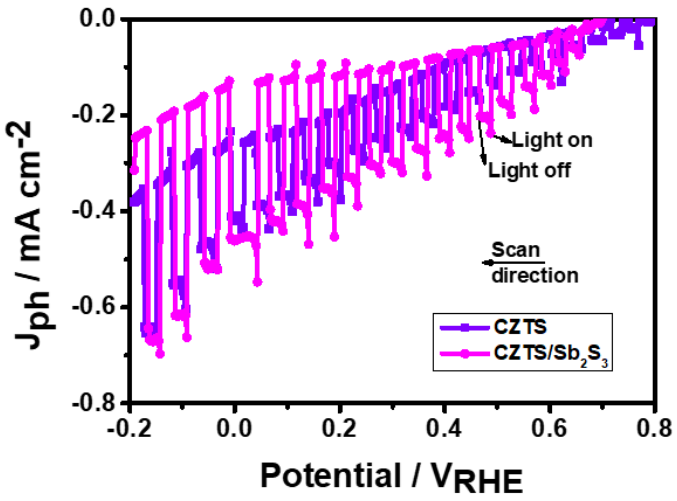

Figure 10: I-E curve of CZTS and CZTS/Sb_2S_3 electrode under chopped illumination under AM 1.5G at the scan rate of 10 mV/sec.

The decrease in dark current suggests that an enhanced heterojunction formation is present. However, the water splitting efficiency considerably declines, indicating that CZTS is inappropriate for usage with Sb_2S_3.

Sb_2S_3/In_2S_3 :

The Sb_2S_3/In_2S_3 heterojunction was fabricated by deposition of FTO in the Sb_2S_3 bath for 5 hr. For the deposition of In_2S_3 over the Sb_2S_3 layer by hydrothermal method, 189.3 mg of Thioacetamide (TAA) was mixed with 281.5 mg $InCl_3.4H_2O$ into the Ethylene glycol solution [59]. The solution was stirred using a magnetic stirrer for 30 minutes, then transferred to an autoclave and heated at 120°C for 4 hours. A thin yellow film formed on the Sb_2S_3 confirms the synthesis of In_2S_3. This synthesis method introduced chloride impurities onto the substrate, which could be disadvantageous for the composite fabrication of Sb_2S_3/In_2S_3. The motivation for using In_2S_3 in the photocathodic system was the report of significant enhancement in the photoanodic current of Sb_2S_3 due to the insertion of the In_2S_3 buffer layer ($FTO/Sb_2S_3/In_2S_3$).

The bare Sb_2S_3 and Sb_2S_3/In_2S_3 electrodes were tested by performing the photocurrent measurements under the chopped illumination of white light. The photocathodic material was subjected to measurement at a scan rate of 10 mv/Sec, over the potential range of -0.2 to 0.8 V (vs. VR_{HE}), under both dark and illuminated conditions. A 0.5 M Na_2SO_4 electrolyte was used with a pH of 6.85, and the area of the photocathode material used as the working electrode was fixed at 0.25 cm^{-2}. Fig. 11 shows that bare Sb_2S_3 exhibits a J_{ph} value of -0.48 mA cm^{-2} at 0 V_{RHE}, while Sb_2S_3/In_2S_3 shows J_{ph} = -0.38 mA cm^{-2} at 0 V_{RHE}. Adding the In_2S_3 layer over Sb_2S_3 leads to a decrease in current density and an increase in the dark current value. Hence, the formation of this composite is not practical via the mentioned synthesis procedure in the PEC Water splitting.

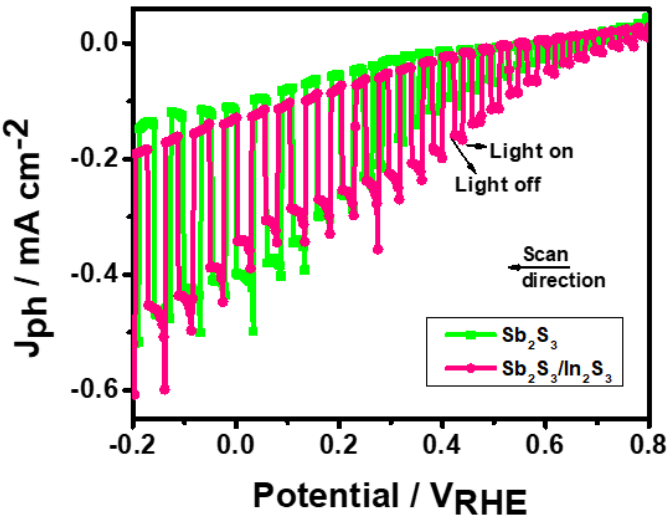

Figure 11: I-E curve of Sb_2S_3 and Sb_2S_3/In_2S_3 electrode under chopped illumination under AM 1.5G at the scan rate of 10 mV/sec.

Chapter 4

Conclusions and Future Perspective

We can conclude that the novel CuO/Sb_2S_3 (-1 mA cm^{-2}) composite was successfully fabricated with the 3 times increase in the J_{ph} value concerning the CuO photocathode (-0.3 mA cm^{-2}). The ABPE efficiency for CuO/Sb_2S_3 and CuO is 0.10% and 0.04%, respectively. Additionally, both CuO and Sb_2S_3 are low-cost, p-type semiconducting materials, making the composite cost-effective. The explanation for the enhancement in the J_{ph} value was given by various instrumentation techniques (UV-vis, EIS, and PL), and for the confirmation of synthesized material, various characterization was done(XRD, SEM, XPS). The developed heterojunction can help in exploring another different composite of oxides-sulfides. The similar band gap of CuO and Sb_2S_3 was disadvantageous for reducing the recombination rate to a greater extent. Hence there is a need to add another layer with a high band gap as compared to these materials, or adding a metal nanoparticle will also be advantageous as it will help in charge separation in a significant way due to its property to show Surface Plasmon Resonance (SPR), future studies will be done by considering these things. The CuO is well explored in the literature, and it is a remarkable photocathodic material, using Sb_2S_3 as a sensitizer, in this case, allows exploring chalcogenides for stabilizing CuO photocathode. It also gives the understanding to explore cost-effective materials for composite formation with CuO compared to using costly buffer layers like Ga_2O_3 and RuO_x as a cocatalyst.

References

[1] A. Kudo and Y. Miseki, "Heterogeneous photocatalyst materials for water splitting," *Chem. Soc. Rev.*, vol. 38, no. 1, 2009, doi: 10.1039/b800489g.

[2] S. Luber *et al.*, "S 1-state model of the O 2-evolving complex of photosystem II," *Biochemistry*, vol. 50, no. 29, pp. 6308–6311, 2011, doi: 10.1021/bi200681q.

[3] M. Gratzel, "Artificial Photosynthesis: Water Cleavage into Hydrogen and Oxygen by Visible Light," *Acc. Chem. Res.*, vol. 14, no. 12, pp. 376–384, 1981, doi: 10.1021/ar00072a003.

[4] Z. Jin, P. Li, and D. Xiao, "Photoanode-immobilized molecular cobalt-based oxygen-evolving complexes with enhanced solar-to-fuel efficiency," *J. Mater. Chem. A*, vol. 4, no. 29, pp. 11228–11233, 2016, doi: 10.1039/c6ta04607j.

[5] M. G. Walter *et al.*, "Solar water splitting cells," *Chem. Rev.*, vol. 110, no. 11, pp. 6446–6473, 2010, doi: 10.1021/cr1002326.

[6] J. E. Thorne, S. Li, C. Du, G. Qin, and D. Wang, "Energetics at the Surface of Photoelectrodes and Its Influence on the Photoelectrochemical Properties," *J. Phys. Chem. Lett.*, vol. 6, no. 20, pp. 4083–4088, 2015, doi: 10.1021/acs.jpclett.5b01372.

[7] G. Wang, X. Yang, F. Qian, J. Z. Zhang, and Y. Li, "Double-sided CdS and CdSe quantum dot co-sensitized ZnO nanowire arrays for photoelectrochemical hydrogen generation," *Nano Lett.*, vol. 10, no. 3, 2010, doi: 10.1021/nl100250z.

[8] F. Wu *et al.*, "Simultaneous Enhancement of Charge Separation and Hole Transportation in a TiO2–SrTiO3 Core–Shell Nanowire Photoelectrochemical System," *Adv. Mater.*, vol. 29, no. 28, 2017, doi: 10.1002/adma.201701432.

[9] D. Chen and Z. Liu, "Efficient Indium Sulfide Photoelectrode with Crystal Phase and Morphology Control for High-Performance Photoelectrochemical Water Splitting," *ACS Sustain. Chem. Eng.*, vol. 6, no. 9, 2018, doi: 10.1021/acssuschemeng.8b02801.

[10] H. Zhang *et al.*, "Gradient tantalum-doped hematite homojunction photoanode improves both photocurrents and turn-on voltage for solar water splitting," *Nat. Commun.*, vol. 11, no. 1, 2020, doi: 10.1038/s41467-020-18484-8.

[11] A. S. Mary, C. Murugan, and A. Pandikumar, "Uplifting the charge carrier separation and migration in Co-doped CuBi2O4/TiO2 p-n heterojunction photocathode for enhanced photoelectrocatalytic water splitting," *J. Colloid Interface Sci.*, vol. 608, 2022, doi: 10.1016/j.jcis.2021.10.172.

[12] Y. Y. Han, X. L. Lu, S. F. Tang, X. P. Yin, Z. W. Wei, and T. B. Lu, "Metal-Free 2D/2D Heterojunction of Graphitic Carbon Nitride/Graphdiyne for Improving the Hole Mobility of Graphitic Carbon Nitride," *Adv. Energy Mater.*, vol. 8, no. 16, 2018, doi: 10.1002/aenm.201702992.

[13] Y. Wei, X. Chang, T. Wang, C. Li, and J. Gong, "A Low-Cost NiO Hole Transfer Layer for Ohmic Back Contact to Cu2O for Photoelectrochemical Water Splitting," *Small*, vol. 13, no. 39, 2017, doi: 10.1002/smll.201702007.

[14] C. Lo Vecchio *et al.*, "Water splitting with enhanced efficiency using a nickel-based

cocatalyst at a cupric oxide photocathode," *Catalysts*, vol. 11, no. 11, 2021, doi: 10.3390/catal11111363.

[15] B. A. D. Williamson, J. Buckeridge, J. Brown, S. Ansbro, R. G. Palgrave, and D. O. Scanlon, "Engineering Valence Band Dispersion for High Mobility p-Type Semiconductors," *Chem. Mater.*, vol. 29, no. 6, pp. 2402–2413, 2017, doi: 10.1021/acs.chemmater.6b03306.

[16] J. Luo, L. Steier, M. K. Son, M. Schreier, M. T. Mayer, and M. Grätzel, "Cu2O Nanowire Photocathodes for Efficient and Durable Solar Water Splitting," *Nano Lett.*, vol. 16, no. 3, pp. 1848–1857, 2016, doi: 10.1021/acs.nanolett.5b04929.

[17] Y. S. Lee *et al.*, "Atomic layer deposited gallium oxide buffer layer enables 1.2 v open-circuit voltage in cuprous oxide solar cells," *Adv. Mater.*, vol. 26, no. 27, pp. 4704–4710, 2014, doi: 10.1002/adma.201401054.

[18] S. Masudy-Panah, Y. J. K. Eugene, N. D. Khiavi, R. Katal, and X. Gong, "Aluminum-incorporated p-CuO/n-ZnO photocathode coated with nanocrystal-engineered TiO2 protective layer for photoelectrochemical water splitting and hydrogen generation," *J. Mater. Chem. A*, vol. 6, no. 25, 2018, doi: 10.1039/c8ta03027h.

[19] Y. Yang, D. Xu, Q. Wu, and P. Diao, "Cu2O/CuO bilayered composite as a high-efficiency photocathode for photoelectrochemical hydrogen evolution reaction," *Sci. Rep.*, vol. 6, no. September, pp. 1–13, 2016, doi: 10.1038/srep35158.

[20] R. Siavash Moakhar *et al.*, "Photoelectrochemical Water-Splitting Using CuO-Based Electrodes for Hydrogen Production: A Review," *Adv. Mater.*, vol. 33, no. 33, 2021, doi: 10.1002/adma.202007285.

[21] A. A. Dubale *et al.*, "Heterostructured Cu2O/CuO decorated with nickel as a highly efficient photocathode for photoelectrochemical water reduction," *J. Mater. Chem. A*, vol. 3, no. 23, pp. 12482–12499, 2015, doi: 10.1039/c5ta01961c.

[22] Y. Yu, L. Pan, M. Son, M. T. Mayer, and W. Zhang, "Solution-Processed Cu 2 S Photocathodes for Photoelectrochemical Water Splitting," 2018, doi: 10.1021/acsenergylett.7b01326.

[23] Y. C. Lin *et al.*, "Sandwich-Nanostructured n-Cu2O/AuAg/p-Cu2O Photocathode with Highly Positive Onset Potential for Improved Water Reduction," *ACS Appl. Mater. Interfaces*, vol. 11, no. 42, pp. 38625–38632, 2019, doi: 10.1021/acsami.9b11737.

[24] M. S. Prévot *et al.*, "Evaluating Charge Carrier Transport and Surface States in CuFeO2 Photocathodes," *Chem. Mater.*, vol. 29, no. 11, pp. 4952–4962, 2017, doi: 10.1021/acs.chemmater.7b01284.

[25] Y. Oh, W. Yang, J. Tan, H. Lee, J. Park, and J. Moon, "Photoelectrodes based on 2D opals assembled from Cu-delafossite double-shelled microspheres for an enhanced photoelectrochemical response," *Nanoscale*, vol. 10, no. 8, pp. 3720–3729, 2018, doi: 10.1039/c7nr07351h.

[26] S. P. Berglund, F. F. Abdi, P. Bogdanoff, A. Chemseddine, D. Friedrich, and R. Van De Krol, "Comprehensive Evaluation of CuBi2O4 as a Photocathode Material for Photoelectrochemical Water Splitting," *Chem. Mater.*, vol. 28, no. 12, pp. 4231–4242, 2016, doi: 10.1021/acs.chemmater.6b00830.

[27] A. Song *et al.*, "Cu:NiO as a hole-selective back contact to improve the

photoelectrochemical performance of CuBi2O4 thin film photocathodes," *J. Mater. Chem. A*, vol. 7, no. 15, pp. 9183–9194, 2019, doi: 10.1039/c9ta01489f.

[28] Y. X. Yu *et al.*, "Solution-Processed Cu2S Photocathodes for Photoelectrochemical Water Splitting," *ACS Energy Lett.*, vol. 3, no. 4, pp. 760–766, 2018, doi: 10.1021/acsenergylett.7b01326.

[29] X. Feng, R. Li, M. Wang, and Y. Chen, "Switchable synthesis of p- and n-type Cu-In-S grooved pyramid-like microcrystals for unassisted photoelectrochemical water splitting," *J. Mater. Chem. A*, vol. 6, no. 24, pp. 11180–11188, 2018, doi: 10.1039/c8ta02386g.

[30] Z. Liu, X. Lu, and D. Chen, "Photoelectrochemical Water Splitting of CuInS2 Photocathode Collaborative Modified with Separated Catalysts Based on Efficient Photogenerated Electron-Hole Separation," *ACS Sustain. Chem. Eng.*, vol. 6, no. 8, pp. 10289–10294, 2018, doi: 10.1021/acssuschemeng.8b01607.

[31] P. Wu, Z. Liu, M. Ruan, Z. Guo, and L. Zhao, "Cobalt-phosphate modified Fe-Zn 0.2 Cd 0.8 S/CuSbS 2 heterojunction photoanode with multiple synergistic effect for enhancing photoelectrochemical water splitting," *Appl. Surf. Sci.*, vol. 476, 2019, doi: 10.1016/j.apsusc.2019.01.150.

[32] F. Ran, P. Li, X. Yuan, J. Zhang, D. Zhang, and S. Chen, "Fabrication of a Sb2Se3/CuSbS2Heterojunction Photocathode for Photoelectrochemical Water Splitting," *J. Phys. Chem. C*, vol. 126, no. 20, pp. 8581–8587, 2022, doi: 10.1021/acs.jpcc.2c00914.

[33] S. Lee *et al.*, "RGB-Colored Cu(In,Ga)(S,Se) 2 Thin-Film Solar Cells with Minimal Efficiency Loss Using Narrow-Bandwidth Stopband Nano-Multilayered Filters," *ACS Appl. Mater. Interfaces*, vol. 11, no. 10, pp. 9994–10003, 2019, doi: 10.1021/acsami.8b21853.

[34] T. J. Jacobsson, C. Platzer-Björkman, M. Edoff, and T. Edvinsson, "CuInxGa1-xSe2 as an efficient photocathode for solar hydrogen generation," *Int. J. Hydrogen Energy*, vol. 38, no. 35, pp. 15027–15035, 2013, doi: 10.1016/j.ijhydene.2013.09.094.

[35] W. Wang *et al.*, "Device characteristics of CZTSSe thin-film solar cells with 12.6% efficiency," *Adv. Energy Mater.*, vol. 4, no. 7, pp. 1–5, 2014, doi: 10.1002/aenm.201301465.

[36] M. Kumar, A. Dubey, N. Adhikari, S. Venkatesan, and Q. Qiao, "Strategic review of secondary phases, defects and defect-complexes in kesterite CZTS-Se solar cells," *Energy Environ. Sci.*, vol. 8, no. 11, pp. 3134–3159, 2015, doi: 10.1039/c5ee02153g.

[37] K. Feng *et al.*, "Near-infrared-driven water splitting for hydrogen evolution using a Cu2ZnSnS4-based photocathode by the application of upconversion nanoparticles," *Sustain. Energy Fuels*, vol. 4, no. 6, pp. 2669–2674, 2020, doi: 10.1039/d0se00152j.

[38] Z. Xiao, W. Meng, J. V. Li, and Y. Yan, "Distant-Atom Mutation for Better Earth-Abundant Light Absorbers: A Case Study of Cu2BaSnSe4," *ACS Energy Lett.*, vol. 2, no. 1, pp. 29–35, 2017, doi: 10.1021/acsenergylett.6b00577.

[39] D. Shin, T. Zhu, X. Huang, O. Gunawan, V. Blum, and D. B. Mitzi, "Earth-Abundant Chalcogenide Photovoltaic Devices with over 5% Efficiency Based on a Cu2BaSn(S,Se)4 Absorber," *Adv. Mater.*, vol. 29, no. 24, pp. 1–7, 2017, doi:

10.1002/adma.201606945.

[40] R. Kondrotas, C. Chen, and J. Tang, “Sb2S3 Solar Cells,” *Joule*, vol. 2, no. 5, pp. 857–878, 2018, doi: 10.1016/j.joule.2018.04.003.

[41] R. R. Prabhakar, T. Moehl, S. Siol, J. Suh, and S. D. Tilley, “Sb2S3/TiO2Heterojunction Photocathodes: Band Alignment and Water Splitting Properties,” *Chem. Mater.*, vol. 32, no. 17, pp. 7247–7253, 2020, doi: 10.1021/acs.chemmater.0c01581.

[42] H. Guo, Y. Cui, Q. Tian, S. Gao, G. Wang, and D. Pan, “Significantly enhancing grain growth in Cu2ZnSn(S,Se)4 absorber layers by insetting Sb2S3, CuSbS2, and NaSb5S8 thin films,” *Cryst. Growth Des.*, vol. 15, no. 2, pp. 771–777, 2015, doi: 10.1021/cg501589t.

[43] Q. Cai, Z. Liu, C. Han, Z. Tong, and C. Ma, "CuInS2/Sb2S3 heterostructure modified with noble metal cocatalyst for efficient photoelectrochemical water splitting," *J. Alloys Compd.*, vol. 795, pp. 319–326, 2019, doi: 10.1016/j.jallcom.2019.04.312.

[44] M. Kumar, C. Ghosh, B. Meena, and T. Ma, “Sustainable Energy & Fuels transfer for e ffi cient solar water splitting †,” pp. 3961–3974, 2022, doi: 10.1039/d2se00600f.

[45] M. G. T. N. D. *et al.*, “One-pot hydrothermal preparation of Cu 2 O-CuO/rGO nanocomposites with enhanced electrochemical performance for supercapacitor applications,” *Appl. Surf. Sci.*, vol. 449, pp. 474–484, 2018, doi: 10.1016/j.apsusc.2017.12.199.

[46] E. Cárdenas, A. Arato, E. Perez-Tijerina, T. K. Das Roy, G. Alan Castillo, and B. Krishnan, “Carbon-doped Sb2S3 thin films: Structural, optical and electrical properties,” *Sol. Energy Mater. Sol. Cells*, vol. 93, no. 1, pp. 33–36, 2009, doi: 10.1016/j.solmat.2008.02.026.

[47] 5 Nair, Y. Peña, J. Campos, V. M. Garcia, and P. K. Nair, “Chemically Deposited Sb 2 S 3 and Sb 2 S 3-CuS Thin Films Chemically Deposited 5b253 and 5b253-CuS Thin Films,” *J. Electrochem. Soc*, vol. 145, no. 6, p. 2113, 1998, [Online]. Available: www.worldscientific.com

[48] R. Łobiński and Z. Marczenko, “Recent Advances in Ultraviolet-Visible Spectrophotometry,” *Crit. Rev. Anal. Chem.*, vol. 23, no. 1–2, pp. 55–111, 1992, doi: 10.1080/10408349208051647.

[49] K. Gelderman, L. Lee, and S. W. Donne, “Flat-band potential of a semiconductor: Using the Mott-Schottky equation,” *J. Chem. Educ.*, vol. 84, no. 4, pp. 685–688, 2007, doi: 10.1021/ed084p685.

[50] L. Nadjo and J. M. Savéant, “Linear sweep voltammetry: Kinetic control by charge transfer and/or secondary chemical reactions. I. Formal kinetics,” *J. Electroanal. Chem.*, vol. 48, no. 1, pp. 113–145, 1973, doi: 10.1016/S0022-0728(73)80300-6.

[51] B. Y. Chang and S. M. Park, “Electrochemical impedance spectroscopy,” *Annu. Rev. Anal. Chem.*, vol. 3, no. 1, pp. 207–229, 2010, doi: 10.1146/annurev.anchem.012809.102211.

[52] A. Chauhan, “Powder XRD Technique and its Applications in Science and Technology,” *J. Anal. Bioanal. Tech.*, vol. 5, no. 6, 2014, doi: 10.4172/2155-9872.1000212.

[53] A. Erbe *et al., How to probe structure, kinetics, and dynamics at complex interfaces in situ and operando by optical spectroscopy*. Elsevier, 2018. doi: 10.1016/B978-0-12-409547-2.14061-2.

[54] Y. PENG *et al.*, "Preparation of Sb2O3/Sb2S3/FeOOH composite photoanodes for enhanced photoelectrochemical water oxidation," *Trans. Nonferrous Met. Soc. China (English Ed.*, vol. 30, no. 6, pp. 1625–1634, 2020, doi: 10.1016/S1003-6326(20)65325-0.

[55] F. Wang, H. Yang, Y. Zhang, and H. Zhang, "KH2PO4-Assisted Synthesis and Electrochemical Performance of Highly Uniform CuBi2O4 Microspheres Hierarchically Self-Assembled by Nanoparticles," *J. Electron. Mater.*, vol. 46, no. 8, pp. 4774–4783, 2017, doi: 10.1007/s11664-017-5417-9.

[56] D. Li, X. Chen, Y. T. Liu, J. Yu, and B. Ding, "Sb2S3 nanoparticles anchored on SnO2 nanofibers: A high-performance hybrid electrocatalyst toward ammonia synthesis under ambient conditions," *Chem. Commun.*, vol. 55, no. 92, pp. 13892–13895, 2019, doi: 10.1039/c9cc07847a.

[57] U. V. Ghorpade *et al.*, "Unassisted visible solar water splitting with efficient photoelectrodes sensitized by quantum dots synthesized: Via an environmentally friendly eutectic solvent-mediated approach," *J. Mater. Chem. A*, vol. 6, no. 45, 2018, doi: 10.1039/c8ta05901b.

[58] C. Sripan, D. Alagarasan, S. Varadharajaperumal, R. Ganesan, and R. Naik, "Influence of solvent on solution processed Cu2ZnSnS4 nanocrystals and annealing induced changes in the optical, structural properties of CZTS film," *Curr. Appl. Phys.*, vol. 20, no. 8, pp. 925–930, 2020, doi: 10.1016/j.cap.2020.05.003.

[59] J. Zhao *et al.*, "Defects regulation of Sb2S3 by construction of Sb2S3/In2S3 direct Z-scheme heterojunction with enhanced photoelectrochemical performance," *Appl. Surf. Sci.*, vol. 568, no. May, p. 150917, 2021, doi: 10.1016/j.apsusc.2021.150917.